
Sample-Efficient Deep RL with Generative Adversarial Tree Search

Kamyar Azizzadenesheli
 UC Irvine
 kazizzad@uci.edu

Brandon Yang
 Stanford University
 bcyang@stanford.edu

Weitang Liu
 UC Davis
 wetliu@ucdavis.edu

Emma Brunskill
 Stanford University
 ebrun@cs.stanford.edu

Zachary C Lipton
 CMU
 zlipton@cmu.edu

Animashree Anandkumar
 Caltech
 anima@caltech.edu

Abstract

We propose Generative Adversarial Tree Search (GATS), a sample-efficient Deep Reinforcement Learning (DRL) algorithm. While Monte Carlo Tree Search (MCTS) is known to be effective for search and planning in RL, it is often sample-inefficient and therefore expensive to apply in practice. In this work, we develop a Generative Adversarial Network (GAN) architecture to model an environment’s dynamics and a predictor model for the reward function. We exploit collected data from interaction with the environment to learn these models, which we then use for model-based planning. During planning, we deploy a finite depth MCTS, using the learned model for tree search and a learned Q -value for the leaves, to find the best action. We theoretically show that GATS improves the bias-variance trade-off in value-based DRL. Moreover, we show that the generative model learns the model dynamics using orders of magnitude fewer samples than the Q -learner. In non-stationary settings where the environment model changes, we find the generative model adapts significantly faster than the Q -learner to the new environment.

1 Introduction

The earliest and best-publicized applications of deep reinforcement learning (DRL) involve Atari games [33] and the board game of Go [40], where experience is inexpensive since the environments are simulated. In such scenarios, DRL can be combined with Monte-Carlo tree search (MCTS) methods [22, 24] for planning, where the agent executes roll-outs on the simulated environment (as far as computationally feasible) to finds suitable policies. However, for episodic problems where the length of each episode is large, MCTS can be very computationally expensive, e.g. Go. In order to speed up MCTS for Go and learn a effective policy, Alpha Go [40] employs a depth limited MCTS on the Go emulator, where a learned Q function is used to query the value of leaf nodes.

In real-world applications, such as robotics [26] and dialogue systems [27], collecting samples often takes considerable time and effort. In such scenarios, the agent typically cannot access either the environment model or its corresponding simulator. Thus, MCTS cannot be carried out in such scenarios, due to the massive sample complexity. In this work, inspired by Alpha Go, we propose a DRL algorithm which utilizes environment samples to learn a Q function as well as the environment model dynamics to build a simulator on which MCTS can be performed. Interestingly, in the field of psychology, it is widely accepted that humans make decisions in part by similarly imagining the future and deliberating their decisions [38].

Recently, Generative Adversarial Networks (GANs) [16] have emerged as a popular tool for generative modeling, especially in high-dimensional data such as images. Unlike previous approaches to

image generation, which typically produced blurry images due to optimizing an L1 or L2 objective, GANs produces crisp, realistic images. GANs have since been extended for conditional generation, for instance generating an image conditioned on a label [31] and video predictions [30]. Recently, PIX2PIX[19] is proposed as a new GAN architecture for image-to-image translation tasks.

In this work, we propose Generative Adversarial Tree Search (GATS), a sample-efficient DRL algorithm which exploits the benefits of both model-free and model-based learning. We build a new generative architecture to learn model dynamics. For model-based learning, we develop a bounded depth MCTS based algorithm on the learned model dynamics and reward process, and for model-free learning, we use DQN and DDQN [33, 41]. In particular, GATS deploys the MCTS method for planning over a specified depth and uses the estimated Q -function as a value for the leaf state¹. We show that with our new architecture, the generative model can learn model dynamics in a significantly smaller fraction of samples than the Q -learning algorithm.

Generative Dynamics Model (GDM), and Reward Predictor (RP). The states in the Arcade Learning Environment [11, 29] for Atari games consist of images (frames of video). This transition function lends itself to approximation via a conditional GAN trained to predict the next frame based on the previous frames and actions. Inspired by PIX2PIX, we develop a new architecture for GDM to learn model dynamics and generate successor states for RL. We use the Wasserstein metric for the GAN loss as W-GAN [3] and we use the spectral normalization technique [32] to create a stable and adaptive GDM. Since in RL, the agent encounters a non-stationary data distribution, finding the best architecture, loss class, and optimization paradigm for GDM is a challenging task. We have done an extensive study on these choices, which mainly appear in the Appendix. The (RP) is a simple model to predict the expected clipped reward for a given state and action. During GDM training, the estimated Wasserstein distance is low for frequently visited state-action pairs but high for rare or unseen state-action pairs. We expect this distance to increase as the number of visits to a state-action pair decreases. We utilize this behavior to develop a heuristic approximation to optimism-based exploration-exploitation strategies instead of ε -greedy. We empirically show that this modification in GATS exploration results in even better performance and sample complexity.

We theoretically analyze the sources of estimation error in GATS expected return estimator. We study the bias-variance trade-off and show that the bias term in DQN exponentially decays as the variance grows as the depth of MCTS grows. We study the bias in the Q estimate of DQN and DDQN, where we find that GATS, with even one step lookahead (depth one), helps to address negative effects of the bias. This leads to a reduction on the sample complexity of DQN by a factor of 2 on the game Pong. We also find that going to higher depths does not appear to confer significantly more benefits for Pong. We choose the domain Pong for our study due to its fast convergence and multiple game modes and difficulties in the latest ALE environment[29]. The reduced computation time allows us to do extensive study of the bias-variance of Q , the effects of different model-based planning and exploration strategies, and domain transfer for the GDM.

Finally, in this work, we developed a new OpenAI gym [13]-like interface for the latest ALE environment[29], which supports different modes and difficulties for each game. In order to study the sample complexity on changing game dynamics, we train GDM and RP on one mode of a given game and we change the environment mode and difficulty. We show that GDM and RP adapts to the new environment in a small number of samples, but it takes an order of magnitude more samples for the Q -learning algorithm to adapt. We documented and will open source this wrapper on the latest ALE.

2 Related Work

The exploration-exploitation trade-off is extensively studied in RL literature [23, 12, 4]. The regret analysis of MDPs [20, 8] is investigated, where the Optimism in the Face of Uncertainty (OFU) principle is applied to guarantee a high probability regret upper bound. For Partially Observable MDPs, OFU is shown to provide high probability regret upper bound [7]. Furthermore, more general settings like partial monitoring games are theoretically tackled [9] and minimax regret guarantees with polynomial dependency in certain dimensions of the problem are provided.

¹One can adapt GATS by choosing another DRL algorithm or planning method (e.g. UCT, MCTS, Policy Gradient)

While theoretical RL addresses the trade-off in exploration-exploitation, this problem is still prominent in empirical reinforcement learning research [33, 1, 6]. On the empirical side, recent success in video games has sparked a flurry of research interest. For example [14, 15, 43] investigate DRL for dialogue policy learning, with [28] addressing the efficiency of exploration. To combat the sample complexity shortcoming, designing an efficient exploration strategy in DRL has emerged as an active research topic, e.g. optimism [37] and Thompson Sampling [36, 28, 5].

Minimizing the Bellman residual using Bootstraps of the Q -function has been the core of value based DRL methods [33, 41]. It has been extensively studied that minimizing the Bellman residual provides a biased estimator of the value function [2]. In order to mitigate this bias, along with other reasons, DQN proposes to update the target value less frequently than the rest of the model in order to mimic the Fitted- Q update. This tweak reduces the bias in the value estimator but significantly increases the sample complexity. On the other hand, Monte Carlo sampling strategies [22, 24] have been proposed as efficient methods for planning, but suffer from high sample complexity in real world applications.

Recently, there have been studies of conditional video prediction for video games [34], where large model is trained with the L2 loss in order to predict long future trajectories of frames given actions. The quality of the generated frames is measured by training DQN on them. Since this model uses $L2$ loss, it suffers to produce reasonable frames in stochastic environments or when the frames contain high frequency modes. Moreover, for deterministic environments, we implemented this work and compared it against GDM. We observe that GDM requires significantly fewer iteration to converge to perceptually good frames with smaller deviation in Q values (Q -function applied on real frames and generated frames) for GATS.

Learned environment models are leveraged in [42], where an encoder model is used to encode the generated trajectories into an abstract representation, which is used as an additional input to the policy model. They validate their methods on a small puzzle world, Sokoban, and, further, show the capability of their model on multi-task learning in their miniPacman environment. [42] does not use explicit planning and roll-out strategies. Further work employs transition models in to perform roll-outs in the encoded state representation [35], and demonstrate modest gains in performance on Atari games (compared to DQN). In contrary, in this work, we are able to learn model dynamics in the original state space, and we demonstrate significant empirical improvement in sample complexity.

Despite GANs' capabilities in recovering the input data manifold and generating perceptually good images, they are difficult to train and often unstable, especially for non-stationary tasks like RL. In recent years, there has been significant progress in developing stable learning procedures. The Wassestien GAN (W-GAN) [3] uses the Wasserstein metric as a notion of distance between two distributions, while requires the discriminator to be from the set of bounded lipschitz functions. In order to satisfied this boundedness, improved W-GAN [17] is proposed which penalizes the discriminator's gradient while found still hard to train. Spectral normalization of discriminators [32] has been studied, where a smooth convergence is empirically observed. We leverage these advances in creating a stable learning procedure for the GDM for RL.

3 Preliminaries

An infinite horizon γ -discounted MDP M is a tuple $\langle \mathcal{X}, \mathcal{A}, T, R, P_0, \gamma \rangle$, with state space \mathcal{X} , action space \mathcal{A} , and P_0 , the distribution over the initial states. The transition kernel $T : x, a \rightarrow \Delta_x$, drives the model dynamics accompanied with $[0, 1]$ -bounded reward of $R : x, a \rightarrow \Delta_r$, where $0 \leq \gamma < 1$. The agent's objective is finding a policy $\pi := \mathcal{X} \rightarrow \mathcal{A}$ that maximizes the overall expected discounted reward $\eta^* := \eta(\pi^*) = \max_{\pi} \lim_{N \rightarrow \infty} \mathbb{E}_{\pi} \left[\sum_{t=0}^N \gamma^t r_t | x_0 \sim P_0 \right]$. Let $Q_{\pi}(x, a) := \lim_{N \rightarrow \infty} \mathbb{E}_{\pi} \left[\sum_{t=0}^N \gamma^t r_t | x_0 = x, a_0 = a \right]$ denote the average discounted reward under policy π starting from state-action x, a . One can learn the Q function in order to find the optimal action at any state. For a given pair of state and action (x, a) , we actually aim to minimize

$$(Q(x, a) - \mathbb{E}_{\pi} [r + \gamma Q(x', a') | x, a])^2 \quad (1)$$

In order to minimize the objective of Eq. 1, a double sampling is required to estimate the inner expectation. To avoid the cost of the double sampling, a common approach is to, instead, minimize

the Bellman residual [25, 2]

$$\mathbb{E}_\pi[(Q(x, a) - (r + \gamma Q(x', a')))^2 | x, a] = (Q(x, a) - \mathbb{E}_\pi[r + \gamma Q(x', a') | x, a])^2 + \text{Var}_\pi(r + \gamma Q(x', a') | x, a)$$

Minimizing the Bellman residual is equivalent to minimizing Eq. 1 and an undesirable additional variance term. DQN partially addresses this bias², by deploying the notion of target value,

$$\mathcal{L}(Q, Q^{\text{target}}) = \mathbb{E}_\pi[(Q(x, a) - r - \gamma Q^{\text{target}}(x', \hat{a}))^2] \quad (2)$$

Generally, in addition to this bias, there is an additional statistical bias due to limited capacity of network, optimization algorithm, and model mismatch to be considered. In the next section, we theoretically and empirically study this bias and show how GATS addresses this undesirable effect. For the dynamic generative model, we propose a generic GDM which consists of a generator G and a discriminator D , trained adversarially w.r.t. the extended conditional Wasserstein metric.

$$W(\mathbb{P}_\varpi, \mathbb{P}_G | \mathbb{P}) := \sup_{D \in \|\cdot\|_L} \mathbb{E}_{\varpi \sim \mathbb{P}_\varpi | \varrho, \varrho \sim \mathbb{P}}[D(\varpi | \varrho)] - \mathbb{E}_{\varpi: G(\varrho \sim \mathbb{P}, z \sim \mathcal{N}(0, I))}[D(\varpi | \varrho)] \quad (3)$$

Here z is a mean-zero unit-variance Gaussian vector random variable and $\|\cdot\|_L$ indicates space of all Lipschitz-1 functions. In GDM, D solves the interior sup, while G 's objective is to minimize this distance and learn the $\mathbb{P}_\varpi | \varrho$ for all ϱ . We deploy our proposed GDM in GATS where \mathbb{P} is the distribution over pairs of $\varrho : (x, a)$ in the replay buffer, and $\mathbb{P}_\varpi | \varrho$ is the distribution over the successor states $\varpi : x'$, which is the transition kernel $T(x' | x, a)$.

4 Generative Adversarial Tree Search

We propose Generative Adversarial Tree Search (GATS) as a (more) sample-efficient DRL algorithm. GATS builds upon DQN and DDQN by reusing the experiences in the replay buffer to learn a reward model RP and model dynamics GDM. Afterward, GATS deploys bounded depth Monte Carlo tree search on the learned model (GDM and RP), instead of the real environment for planning. It then uses the learned Q -function to estimate the maximum expected return at the leaf nodes Fig. 6. In order to learn the model dynamics, we propose GDM, parametrized by θ^{GDM} , as an extension to the architecture of PIX2PIX, an image to image translation model [19]. The input to GDM is the state (four consecutive frames) and a sequence of actions, from which GDM generates the successor frames. We train GDM by sampling mini-batches of experiences from the replay buffer. Simultaneously, we train RP, parameterized with θ^{RP} , using samples from the replay buffer.

Bias and Variance trade-off. In the previous sections, we studied the objective function used in DQN, Eq. 2, which is inherently a biased estimator. In the next section, we show how big these biases can be in practice. Moreover, in addition to DQN and statistical biases, the learned Q can suffer from variance due to low samples regime in the sequential regressions defined in DQN. Let e_Q denote the upper bound on estimation error in Q function; $|Q(x, a) - \tilde{Q}(x, a)| \leq e_Q, \forall x, a$, where $\tilde{Q}(x, a) = \mathbb{E}[r + \max_{a'} Q(x', a')]$. For a given roll-out policy π_r , using GDM, RP, and estimated Q , the expected return $\xi_p(\pi_r, x)$ (the subscript p stands for predicted)

$$\xi_p(\pi_r, x) := \mathbb{E}_{\pi_r, \text{GDM}, \text{RP}} \left[\left(\sum_{h=0}^{H-1} \gamma^h \hat{r}_h \right) + \gamma^H \max_a \hat{Q}(\hat{x}_H, a) | x \right] \quad (4)$$

Since this expectation is not under the real environment, given GDM, RP and Q estimate, GATS efficiently estimates this expected return without any interaction with the real environment. Let $\xi(\pi_r, x)$ denote the same quantity under the ground truth model

$$\xi(\pi_r, x) := \mathbb{E}_{\pi_r} \left[\left(\sum_{h=0}^{H-1} \gamma^h r_h \right) + \gamma^H \max_a \tilde{Q}(\hat{x}_H, a) | x \right]$$

Moreover, for the RP and GDM, where \hat{T} is the estimated transition kernel³ $\forall x, x', \hat{x}, \hat{x}', a \in \mathcal{X}, \mathcal{A}$

$$\sum_a |(r(x, a) - \hat{r}(\hat{x}, a))| \leq e_R, \text{ and, } \sum_{x'} |(T(x' | x, a) - \hat{T}(\hat{x}' | x, a))| \leq e_T$$

²This bias vanishes in deterministic domains

³In the latter sections, we emphatically study e_R and e_T , Fig. 5 and observe that they are surprisingly small in practice, e.g. RP, on average, makes less than two mistakes per entire episode in Pong

Theorem 1. [Bias-Variance trade-off] If GATS is run to estimate the Q function using DQN procedure with the learned model of the environment from GDM and RP, then the deviation in estimating $\xi_p(\pi_r, x) \forall x$ and π_r is bounded as;

$$|\xi_p(\pi_r, x) - \xi(\pi_r, x)| \leq \gamma^H e_Q + \frac{\gamma^H}{1-\gamma} H e_T + \frac{1-\gamma^H}{1-\gamma} (e_T + e_R) \quad (5)$$

Proof. We decompose the error in estimation $\xi_p(\pi_r, x)$, RHS of Eq. 4. The first term in estimation of $\xi_p(\pi_r, x)$, RHS of Eq. 4 carries an error in modeling of the environment and depends on the deficiency in the perfectness of RP and GDM models, second part is mostly due to the bias and variance in DQN estimate of Q -function e_Q as well as the GDM due to the distribution shift in \hat{x}_H . Therefore, for the second term, by adding and subtraction this term, $\mathbb{E}_{\pi_r}[\gamma^H \max_a \hat{Q}(\hat{x}_H, a)]$, we have;

$$\begin{aligned} & \left| \mathbb{E}_{\pi_r, \text{GDM, RP}} \left[\gamma^H \max_a \hat{Q}(\hat{x}_H, a) \middle| x \right] - \mathbb{E}_{\pi_r} \left[\gamma^H \max_a Q(x_H, a) \middle| x \right] \right| \\ & \leq \gamma^H e_Q + \frac{\gamma^H}{1-\gamma} \sum_{x_H} \left| P(x_H|x, \pi_r) - \hat{P}(\hat{x}_H|x, \pi_r) \right| \end{aligned} \quad (6)$$

The term $\frac{1}{1-\gamma}$ appears due to the fact that the maximum possible Q is not greater than $\frac{1}{1-\gamma}$. In order to bound $\left| P(x_H|x, \pi_r) - \hat{P}(\hat{x}_H|x, \pi_r) \right|$, we need to expand them even further. For instance, for $P(x_H|x, \pi_r)$, we have

$$P(x_H|x, \pi_r) := \sum_{x_i, a_i, \forall i \in [1,..,H-1]} T(x_i|x, a_i) \pi_r(a_1|x) \prod_{i=2}^{H-1} T(x_i|x_{i-1}, a_i) \pi_r(a_i|x_{i-1}) T(x_H|x_{H-1}, a_H) \pi_r(a_H|x_{H-1})$$

Again, with adding and subtracting trick, the difference can be written as follows;

$$\begin{aligned} \sum_{x_H} \left| P(x_H|x, \pi_r) - \hat{P}(\hat{x}_H|x, \pi_r) \right| &= \sum_{x_i, a_i, \forall i \in [H]} \left| T(x_1|x, a_1) - \hat{T}(\hat{x}_1|x, a_1) \right| \pi_r(a_1|x) \prod_{i=2}^H T(x_i|x_{i-1}, a_i) \pi_r(a_i|x_{i-1}) \\ &+ \sum_{j=2}^H \sum_{x_h, a_h, \forall i \in [H]} \left(\hat{T}(\hat{x}_1|x, a_1) \right) \pi_r(a_1|x) \left| T(x_j|x_{j-1}, a_j) - \hat{T}(\hat{x}_j|x_{j-1}, a_j) \right| \\ &\quad \prod_{h=2}^{j-1} T'(\hat{x}_h|x_{h-1}, a_h) \pi_r(a_h|\hat{x}_{i-1}) \prod_{h=j+1}^H T(x_h|x_{h-1}, a_h) \pi_r(a_h|x_{h-1}) \end{aligned}$$

Since e_T is the bound on the transition kernel estimate;

$$\sum_{x_H} \left| P(x_H|x, \pi_r) - \hat{P}(\hat{x}_H|x, \pi_r) \right| \leq H e_T$$

Now, we can interpret that GATS significantly (exponentially in depth) reduces the bias and variance, in Q estimate, as $\gamma^H e_Q$. At the same time, since the maximum possible Q is less than or equal to $\frac{1}{1-\gamma}$, the error in the second term of Eq. 6 from GDM decreases as $\frac{\gamma^H}{1-\gamma} H e_T$. Another source of error in estimating $\xi_p(\pi_r, x)$ comes from the first term in the right hand side of Eq. 4, which is due to deficiency in the RP and GDM models.

$$\left| \mathbb{E}_{\pi_r, \text{GDM, RP}} \left[\sum_{h=0}^{H-1} \gamma^h \hat{r}_h \right] - \mathbb{E}_{\pi_r} \left[\sum_{h=0}^{H-1} \gamma^h r_h \right] \right|$$

In order to bound this quantity, we use the same decomposition procedure and;

$$\left| \mathbb{E}_{\pi_r, \text{GDM, RP}} \left[\sum_{h=0}^{H-1} \gamma^h \hat{r}_h \right] - \mathbb{E}_{\pi_r} \left[\sum_{h=0}^{H-1} \gamma^h r_h \right] \right| \leq \sum_i^{H-1} \gamma^i e_T + \sum_i^{H-1} \gamma^i e_R = \frac{1-\gamma^H}{1-\gamma} (e_T + e_R)$$

Thm. 1 provides an insight into the contribution of each source of error into the GATS predicted expected return $\xi_p(\pi_r, x)$. The exponential vanishing error in Q estimates comes at the cost of variances in the model estimation. Therefore, the agent can choose H , the depth of roll-out, in such a way to minimize the estimation error. \square

Algorithm 1 GATS (H)

```

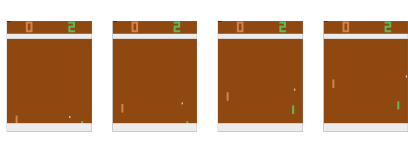
1: Initialize parameter sets  $\theta, \theta', \theta^{target}, \theta^{GDM}, \theta^{RP}$ 
2: Initialize replay buffer and set counter = 0
3: for episode = 1 to inf do
4:   for  $t$  = to the end of episode do
5:      $a_t = MCTS(x_t, H, \theta, \theta^{GDM}, \theta^{RP})$ 
6:     Store transition  $(x_t, a_t, r_t, x_{t+1})$  in replay buffer
7:     Sample a random minibatch of transitions  $(x_\tau, a_\tau, r_\tau, x_{\tau+1})$  from replay buffer
8:      $y_\tau \leftarrow \begin{cases} r_\tau & \text{for terminal } x_{\tau+1} \\ r_\tau + \max_{a'} Q(x_{\tau+1}, a'; \theta^{target}) & \text{for non-terminal } x_{\tau+1} \end{cases}$ 
9:      $\theta \leftarrow \theta - \eta \cdot \nabla_\theta (y_\tau - Q(x_\tau, a_\tau; \theta))^2$ 
10:     $\theta' \leftarrow \theta' - \eta \cdot \nabla_{\theta'} (y_\tau - Q(\hat{x}_\tau, a_\tau; \theta'))^2$ 
11:    Update GDM, and RP
12:  end for
13: end for

```

5 Experiments

We extensively study the performance of GATS on a Atari-like game *Pong* using OpenAI Gym [13]. The DQN architecture and the game design choices are fully borrowed from [33]. The architecture of GDM extends the proposed U-Net model for the generator inspired by the PIX2PIX network [19]. The GDM receives a state, sequence of actions, and a Gaussian noise ⁴ and outputs the next state.⁵ The RP is a simple model with 3 outputs, one for each possible clipped reward. We train GDM and RP using weighted mini-batches of size 128 (more weight on recent samples), and update the two networks every 16 decision steps of GATS (4 times less frequently than the Q update). We deploy GATS as bounded-depth Monte Carlo tree search on the learned model ⁶ and use the learned Q values at the leaves.

Bias-Variance of Q_θ . To observe the existing bias and variance in Q_θ , we run solely DQN on the game Pong, for $20M$ time steps. Fig. 1 shows 4 consecutive frames where the agent receives a negative score and Table. 1 shows the estimated Q values by DQN for these steps. As we observe in Fig. 1 and Table. 1, at the time step t , the estimated Q value of all the actions are almost the same. The agent takes the *down* action and the environment goes to the next state $t + 1$. The second row of Table. 1 expresses the Q value of the actions at this new state. Since this transition does not carry any reward and the discount factor is close to 1, ($\gamma = 0.99$) we expect the max Q values at time step $t + 1$ to be close the Q values of action *down*, but it is very different.



Action space		
Steps	stay	up
t	4.3918	4.3220
$t + 1$	2.7985	2.8371
$t + 2$	2.8089	2.8382
$t + 3$	3.8725	3.8795

Figure 1: The sequence of four consecutive decision states, and corresponding learned Q function by DQN at $t, t + 1, t + 2, t + 3$ from left to right, where the agent loses the point.

Moreover, in Fig. 2 and Table. 2 we investigate the case that the agent catches the ball. The ball is going to the right and agent needs to catch it. At time step t , the paddle is not on the direction of ball velocity, and as shown in Table. 2, the optimal action is *down*. But a closer look at the estimated Q value of action *up* reveals that the Q value for both action *up* is unreasonably close, when it could lead to losing the point. Lastly, we studied the existing errors in the estimation of the Q function using DQN. In Table.1, if the agent could roll-out even one step before making a decision, it could

⁴We set the noise to zero for deterministic environments.

⁵See Apx for detailed explanation on architecture and optimization procedure.

⁶Note that MCTS in a deterministic environment corresponds to lookahead tree search.

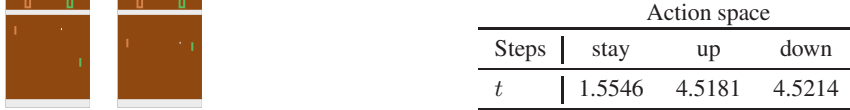


Figure 2: States at $t - 1 \rightarrow t$ and the corresponding Q function learned through DQN at time t .

observe negative consequence of action *down*. The positive effect of the roll-out is more significant in earlier stages of Q learning, where the Q estimation is more off.

We run GATS with 1, 2, 3, and 4 steps lookahead (*GATS1*, *GATS2*, *GATS3*, *GATS4*) and show its performance improvement over DQN in Fig. 3*left*. Fig. 3*right* shows the RP prediction accuracy. We observe that when the transition phase occurs at decision step 1M, the RP model mis-classifies the positive rewards. But the RP rapidly adapts to this shift and reduces the classification error to less than 2 errors per episode. As DRL methods are data hungry, we can re-use the data to efficiently learn the model dynamics. Fig. 5 shows how accurate the GDM can generate next 9 frames just conditioning on the first frame and the trajectory of actions. This trajectory is generated at decision step 100k. In addition to GATS on DQN, we also study two other set of experiments on DDQN.

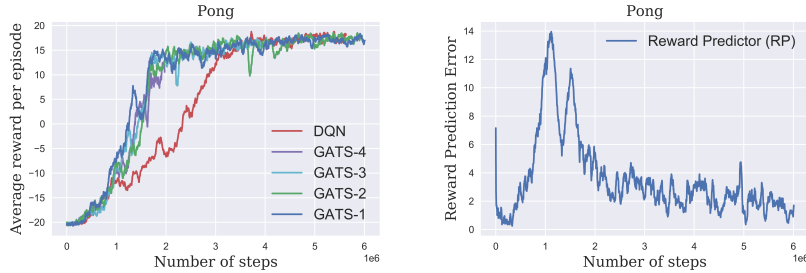


Figure 3: *left*:GATS learns a better policy faster than plain DQN (2 times faster). GATS k denotes GATS of depth k . *right*: Accuracy of RP. The Y axis shows the number of mistakes per episode and each episode has average length of $2k$, so the acc is almost always around 99.8%. This accuracy is consistent among runs and different lookahead lengths.

Since Fig. 3 shows that the deeper roll-outs beyond one step do not provide much additional benefit for Pong, we focus on one-step roll-outs for the next two experiments. In the first experiment, we propose a new optimism-based exploration for GATS. An interesting property of the Wasserstein metric is that over GDM training, this distance decreases for frequently seen state-action experiences and stays high for rare experiences. Intuitively, for unfamiliar experiences, the generator is unable to generate a suitable frame to fool the discriminator, so the Wasserstein distance is high. We can use this distance as an approximation to a decreasing function of inverse pseudo count (also count for finite state MDP) over the experiences, i.e. $1/\tilde{N}(x, a)$. As it is theoretically investigated in Upper Confidence bound RL (UCRL), an OFU based analysis of MDPs [20], we can use this pseudo count to approximate the optimism over the learned Q function. The optimistic Q , \tilde{Q} is as follows:

$$\tilde{Q}_\pi(x, a) = \hat{r}(x, a) + c\sqrt{\log(T)/\tilde{N}(x, a)} + \gamma \sum_{x'} \hat{T}(x'|x, a) \tilde{Q}_\pi(x', \pi(x')) \quad (7)$$

where T is horizon time, and c is a confidence scale constant. We can decouple Eq. 7 in the Q learning and confidence learning parts, i.e. $\tilde{Q}_\pi(x, a) = Q_\pi(x, a) + C_\pi(x, a)$

$$C_\pi(x, a) := c\sqrt{\log(T)/\tilde{N}(x, a)} + \gamma \sum_{x'} \hat{T}(x'|x, a) C_\pi(x', \pi(x')) \quad (8)$$

Therefore, we can learn C , the same way as we learn Q by using DDQN. Since we do not have access to the counts and also not able to do Q-learning, we, heuristically, substitute $c\sqrt{\log(T)/\tilde{N}(x, a)}$ with the scaled Wasserstein distance at (x, a) and approximate the C function. Therefore, we deploy this learned confidence and add it to $\hat{\xi}(\pi_r, x)$ for our GATS planning, i.e. $\max_\pi \{\hat{\xi}(\pi_r, x) + C(\pi_r, x)\}$. This heuristic approach encourages the agent to explore the parts of state space where the GDM does not perform well. If those parts of the state space correspond to less frequently

visited parts of the state space, then this can help with better exploration compared to ε -greedy approach. Therefore, we equip GATS +DDQN with the mentioned optimism approach, and compare it with DDQN and plain GATS, which both use ε -greedy based approaches for exploration. In Fig. 4*left*, we observe that this optimism heuristic is helpful for better exploration.

In the second experiment, we investigate the effect of prioritizing training samples for the GDM by recency, which we do in all experiments reported in Fig. 4*left*. We study the case where the input samples to GDM are instead chosen uniformly at random from the replay buffer in Fig. 4*right*. In this case the GATS learns a better policy faster at the beginning of the game, but the performance stays behind DDQN, due to the shift in the state distribution. It is worth mentioning that for optimism based exploration, there is no ε -greedy, which is why it gets close to the maximum score of 21. We tested DDQN and GATS-DDQN with $\varepsilon = 0$, and they also perform close to 21.

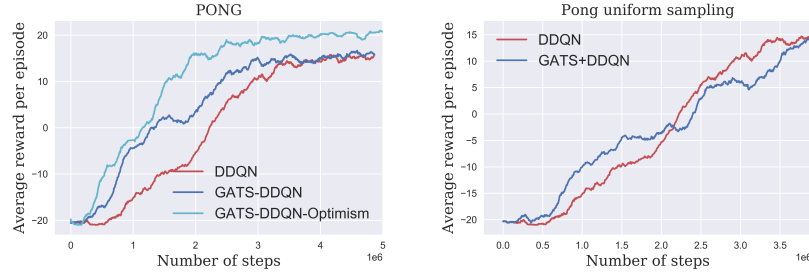


Figure 4: *left*: The optimism approach for GATS improves the sample complexity and learns a better policy faster. *right*: Sampling the replay buffer uniformly at random to train GDM, makes GDM slow to adapt to novel parts of state space.

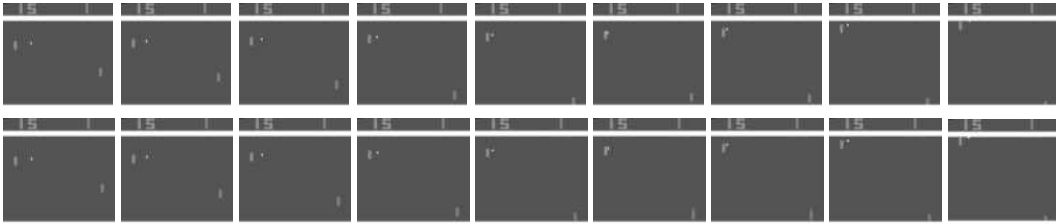


Figure 5: First row: A sequence of real frames. Second row: a corresponding sequence of generated frames

6 Discussion

One notable aspect of the GATS algorithm is its flexibility. GATS consists of a few building blocks: *(i)* Value learning; we deployed DQN and DDQN, *(ii)* Planning; we use pure Monte Carlo sampling, *(iii)* Reward predictor; we used a simple 3-class classifier; *(iv)* Model dynamics, we propose the GDM architecture. Practically, one can easily deploy any other methods for each of these blocks. For instance, for value learning *(i)*, one can use Count-based methods[10]. For planning *(ii)*, one can use upper confidence bound tree search (UTC)[24] or policy gradient methods [21, 39]. For the reward model *(iii)*, if the reward has a continuous distribution, one can learn the mean reward using any regression model. Lastly, for model dynamics *(iv)*, one can extend GDM or choose any other image generating model. Interestingly, this work can be extended to the λ -return setting, where a mix of n steps are acquired. This freedom in the GATS design allows easy adaptation to different domains and problems, and provides many avenues for further exploration. While GATS provides many advantages is a flexible RL paradigm, it suffers from the computation cost due to MCTS. This overhead can be relaxed by parallelization or distilled policy method [18] through a smaller network, which are not the focus of this work.

7 Acknowledgments

K. Azizzadenesheli is supported in part by NSF Career Award CCF-1254106 and Air Force FA9550-15-1-0221. A. Anandkumar is supported in part by Microsoft Faculty Fellowship, Google Faculty Research Award, Adobe Grant, NSF Career Award CCF-1254106, and AFOSR YIP FA9550-15-1-0221.

References

1. D. Abel, A. Agarwal, F. Diaz, A. Krishnamurthy, and R. E. Schapire. Exploratory gradient boosting for reinforcement learning in complex domains. *arXiv*, 2016.
2. A. Antos, C. Szepesvári, and R. Munos. Learning near-optimal policies with bellman-residual minimization based fitted policy iteration and a single sample path. *Machine Learning*, 2008.
3. M. Arjovsky, S. Chintala, and L. Bottou. Wasserstein gan. *arXiv preprint arXiv:1701.07875*, 2017.
4. J. Asmuth, L. Li, M. L. Littman, A. Nouri, and D. Wingate. A bayesian sampling approach to exploration in reinforcement learning. In *Proceedings of the Twenty-Fifth Conference on Uncertainty in Artificial Intelligence*, 2009.
5. K. Azizzadenesheli, E. Brunskill, and A. Anandkumar. Efficient exploration through bayesian deep q-networks. *arXiv preprint arXiv:1802.04412*, 2018.
6. K. Azizzadenesheli, A. Lazaric, and A. Anandkumar. Reinforcement learning in rich-observation mdps using spectral methods. *arXiv preprint arXiv:1611.03907*, 2016.
7. K. Azizzadenesheli, A. Lazaric, and A. Anandkumar. Reinforcement learning of pomdps using spectral methods. In *Proceedings of the 29th Annual Conference on Learning Theory (COLT)*, 2016.
8. P. L. Bartlett and A. Tewari. REGAL: A regularization based algorithm for reinforcement learning in weakly communicating MDPs. In *Proceedings of the 25th Annual Conference on Uncertainty in Artificial Intelligence*, 2009.
9. G. Bartók, D. P. Foster, D. Pál, A. Rakhlin, and C. Szepesvári. Partial monitoring—classification, regret bounds, and algorithms. *Mathematics of Operations Research*, 2014.
10. M. Bellemare, S. Srinivasan, G. Ostrovski, T. Schaul, D. Saxton, and R. Munos. Unifying count-based exploration and intrinsic motivation. In *Advances in Neural Information Processing Systems*, pages 1471–1479, 2016.
11. M. G. Bellemare, Y. Naddaf, J. Veness, and M. Bowling. The arcade learning environment: An evaluation platform for general agents. *J. Artif. Intell. Res.(JAIR)*, 2013.
12. R. I. Brafman and M. Tennenholtz. R-max-a general polynomial time algorithm for near-optimal reinforcement learning. *The Journal of Machine Learning Research*, 3:213–231, 2003.
13. G. Brockman, V. Cheung, L. Pettersson, J. Schneider, J. Schulman, J. Tang, and W. Zaremba. Openai gym, 2016.
14. H. Cuayáhuitl. Simpaleds: A simple deep reinforcement learning dialogue system. *arXiv:1601.04574*, 2016.
15. M. Fatemi, L. E. Asri, H. Schulz, J. He, and K. Suleman. Policy networks with two-stage training for dialogue systems. *arXiv:1606.03152*, 2016.
16. I. Goodfellow, J. Pouget-Abadie, M. Mirza, B. Xu, D. Warde-Farley, S. Ozair, A. Courville, and Y. Bengio. Generative adversarial nets. In *Advances in neural information processing systems*, pages 2672–2680, 2014.

17. I. Gulrajani, F. Ahmed, M. Arjovsky, V. Dumoulin, and A. C. Courville. Improved training of wasserstein gans. In *Advances in Neural Information Processing Systems*, pages 5769–5779, 2017.
18. X. Guo, S. Singh, H. Lee, R. L. Lewis, and X. Wang. Deep learning for real-time atari game play using offline monte-carlo tree search planning. In *Advances in neural information processing systems*, pages 3338–3346, 2014.
19. P. Isola, J.-Y. Zhu, T. Zhou, and A. A. Efros. Image-to-image translation with conditional adversarial networks. *arXiv preprint*, 2017.
20. T. Jaksch, R. Ortner, and P. Auer. Near-optimal regret bounds for reinforcement learning. *Journal of Machine Learning Research*, 2010.
21. S. M. Kakade. A natural policy gradient. In *Advances in neural information processing systems*, 2002.
22. M. Kearns, Y. Mansour, and A. Y. Ng. A sparse sampling algorithm for near-optimal planning in large markov decision processes. *Machine Learning*, 49(2-3):193–208, 2002.
23. M. Kearns and S. Singh. Near-optimal reinforcement learning in polynomial time. *Machine Learning*, 49(2-3):209–232, 2002.
24. L. Kocsis and C. Szepesvári. Bandit based monte-carlo planning. In *Machine Learning: ECML 2006*, pages 282–293. Springer, 2006.
25. M. G. Lagoudakis and R. Parr. Least-squares policy iteration. *Journal of machine learning research*, 4(Dec):1107–1149, 2003.
26. S. Levine et al. End-to-end training of deep visuomotor policies. *JMLR*, 2016.
27. Z. C. Lipton, K. Azizzadenesheli, J. Gao, L. Li, J. Chen, and L. Deng. Combating reinforcement learning’s sisyphean curse with intrinsic fear. *arXiv preprint arXiv:1611.01211*, 2016.
28. Z. C. Lipton, J. Gao, L. Li, X. Li, F. Ahmed, and L. Deng. Efficient exploration for dialogue policy learning with bbq networks & replay buffer spiking. *AAAI*, 2018.
29. M. C. Machado, M. G. Bellemare, E. Talvitie, J. Veness, M. Hausknecht, and M. Bowling. Revisiting the arcade learning environment: Evaluation protocols and open problems for general agents. *arXiv preprint arXiv:1709.06009*, 2017.
30. M. Mathieu, C. Couprie, and Y. LeCun. Deep multi-scale video prediction beyond mean square error. *arXiv preprint arXiv:1511.05440*, 2015.
31. M. Mirza and S. Osindero. Conditional generative adversarial nets. *arXiv preprint arXiv:1411.1784*, 2014.
32. T. Miyato, T. Kataoka, M. Koyama, and Y. Yoshida. Spectral normalization for generative adversarial networks. *arXiv preprint arXiv:1802.05957*, 2018.
33. V. Mnih, K. Kavukcuoglu, D. Silver, A. A. Rusu, J. Veness, M. G. Bellemare, A. Graves, M. Riedmiller, A. K. Fidjeland, G. Ostrovski, et al. Human-level control through deep reinforcement learning. *Nature*, 2015.
34. J. Oh, X. Guo, H. Lee, R. L. Lewis, and S. Singh. Action-conditional video prediction using deep networks in atari games. In *Advances in Neural Information Processing Systems*, 2015.
35. J. Oh, S. Singh, and H. Lee. Value prediction network. In *Advances in Neural Information Processing Systems*, pages 6120–6130, 2017.
36. I. Osband, C. Blundell, A. Pritzel, and B. Van Roy. Deep exploration via bootstrapped dqn. In *Advances in Neural Information Processing Systems*, 2016.
37. G. Ostrovski, M. G. Bellemare, A. v. d. Oord, and R. Munos. Count-based exploration with neural density models. *arXiv preprint arXiv:1703.01310*, 2017.

38. D. L. Schacter, D. R. Addis, D. Hassabis, V. C. Martin, R. N. Spreng, and K. K. Szpunar. The future of memory: remembering, imagining, and the brain. *Neuron*, 76(4):677–694, 2012.
39. J. Schulman, S. Levine, P. Abbeel, M. Jordan, and P. Moritz. Trust region policy optimization. In *Proceedings of the 32nd International Conference on Machine Learning (ICML-15)*, 2015.
40. D. Silver et al. Mastering the game of go with deep neural networks and tree search. *Nature*, 2016.
41. H. Van Hasselt, A. Guez, and D. Silver. Deep reinforcement learning with double q-learning. In *AAAI*, 2016.
42. T. Weber, S. Racanière, D. P. Reichert, L. Buesing, A. Guez, D. J. Rezende, A. P. Badia, O. Vinyals, N. Heess, Y. Li, et al. Imagination-augmented agents for deep reinforcement learning. *arXiv*, 2017.
43. T.-H. Wen, M. Gasic, N. Mrksic, L. M. Rojas-Barahona, P.-H. Su, S. Ultes, D. Vandyke, and S. Young. A network-based end-to-end trainable task-oriented dialogue system. *arXiv:1604.04562*, 2016.

Appendix

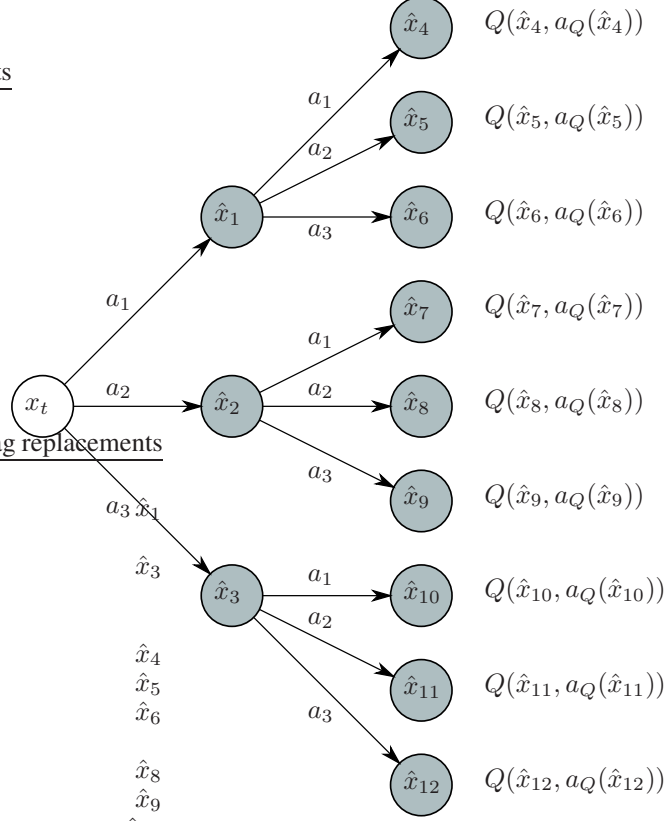


Figure 6: Roll-out of depth two starting from state x_t . Here \hat{x} 's are the generated states by GDM. $Q(x, a(x))$ denotes the predicted value of state x choosing the greedy action $a_Q(x) := \arg \max_{a' \in \mathcal{A}} Q(x, a')$.

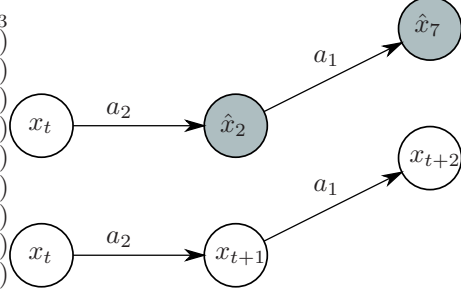


Figure 7: Training GAN and $Q_{\theta'}$ using the longer trajectory of experiences

GDM Architecture and parameters The GDM model consists of seven convolution and also seven deconvolution layers. Each convolution layer is followed by Batch Normalization layers and the leaky RLU activation function with negative slope of -0.2 . Also each deconvolution layer is followed by a Batch Normalization layer and the RELU activation instead of leaky RELU. The encoder part of the network uses channel dimensions of $32, 32, 64, 128, 256, 512, 512$ and kernel sizes of $4, 4, 4, 4, 2, 2, 2$. The reverse is true for the decoder part. We concatenate the bottleneck and next 5 deconvolution layers with a random Gaussian noise of dimension 100, the action sequence, and also the corresponding layer in the encoder. The last layer of decoder is not concatenated. Fig. 8. For the discriminator, instead of convolution, we use SN-convolution³² which ensures the Lipschitz constant of the discriminator is below 1. The discriminator consists of four SN-convolution layers followed by Batch Normalization layers and a leaky RELU activation with negative slope of -0.2 .

The number of channels increase as 64, 128, 256, 16 with kernel size of 8, 4, 4, 3, which is followed by two fully connected layers of size 400 and 18 where their inputs are concatenated with the action sequence. The output is a single number without any nonlinearity. The action sequence uses one hot encoding representation.

We train the generator using Adam optimizer with weight decay of 0.001, learning rate of 0.0001 and also $\text{beta1}, \text{beta2} = 0.5, 0.999$. For the discriminator, we use SGD optimizer with smaller learning rate of 0.00001, momentum of 0.9, and weight decay of 0.1. Given the fact that we use Wasserstein metric for GDM training, the followings are the generator and discriminator gradient updates: for a given set of 5 frames and a action, sampled from the replay buffer, $(f_1, f_2, f_3, f_4, a_4, f_5)$ and a random Gaussian vector z :

Discriminator update:

$$\nabla_{\theta_D} \left[\frac{1}{m} \sum_{i=1}^m D_{\theta_D}(f_5, f_4, f_3, f_2, a_4) - \frac{1}{m} \sum_{i=1}^m D_{\theta_D}(G_{\theta_G}(f_4, f_3, f_2, f_1, a_4), f_4, f_3, f_2, a_4, z) \right]$$

Generator update:

$$\nabla_{\theta_G} \left[-\frac{1}{m} \sum_{i=1}^m D_{\theta_D}(G_{\theta_G}(f_4, f_3, f_2, f_1, a_4, z), f_4, f_3, f_2, a_4) \right]$$

where $\theta^{\text{GDM}} = \{\theta_G, \theta_D\}$ are the generator parameters and discriminator parameters. In order to improve the quality of the generated frames, it is common to also add a class of multiple losses and capture different frequency aspects of the frames^{19,34}. Therefore, we also add $10 * L1 + 90 * L2$ loss to the GAN loss in order to improve the training process. It is worth noting that these losses are defined on the frames with pixel values in $[-1, 1]$, therefore they are small but still able to help speed up the the learning. In order to be able to roll-out for a longer and preserve the GDM quality, we also train the generator using self generated samples, i.e. given the sequence $(f_1, f_2, f_3, f_4, a_4, f_5, a_5, f_6, a_6, f_7, a_7, f_8)$, we also train the generator and discriminator on the generated samples of generator condition on its own generated samples for depth of three. This allows us to roll out for longer horizon of more than 10 and still preserve the GDM accuracy.

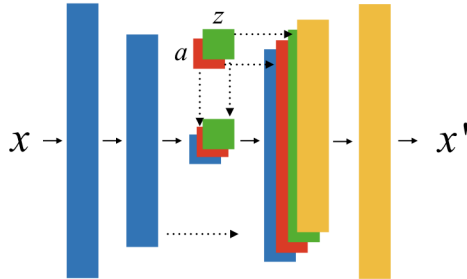


Figure 8: The GDM generator is an encoder-decoder architecture with skip-connections between mirrored layers, with action and Gaussian noise concatenated in the bottleneck and decoder layers.

Q function on generated frames Ideally, if the GDM model is perfect at generating frames i.e. the space generated frames is, pixel by pixel, the same as the real frames, for the leaf nodes x_H , we can use $\max_a Q(x_H, a; \theta)$, learned by the DQN model on real frames, in order to assign values to the leaf nodes. But in practice, instead of x_H , we have access to \hat{x}_H , a generated state that perceptually is similar to x_H (Fig. 5), but from the perspective of Q_θ , they might not be similar over the course of training of Q_θ . In order to compensate for this error, we train another Q -network, parameterized with θ' , in order to provide the similar Q-value as Q_θ for generated frames. To train $Q_{\theta'}$, we minimize the $L2$ norm between $Q_{\theta'}$ and Q_θ for a given GAN sample state and trajectory Fig. 7. For this minimization, we use Adam with learning rate of 0.0001, no weight decay, and $\text{beta1}, \text{beta2} = 0.5, 0.999$. We experimented with weight decay and adding $L1$ loss, but we find these optimizations degrade the performance of the network. We tracked the difference between $Q_\theta(\hat{x}) - Q_\theta(x)$ and $Q_{\theta'}(\hat{x}) - Q_\theta(x)$ and observed that both of these quantities are negligible. We ran GATS without the $Q_{\theta'}$, with just Q_θ , and observed only slightly worse performance.

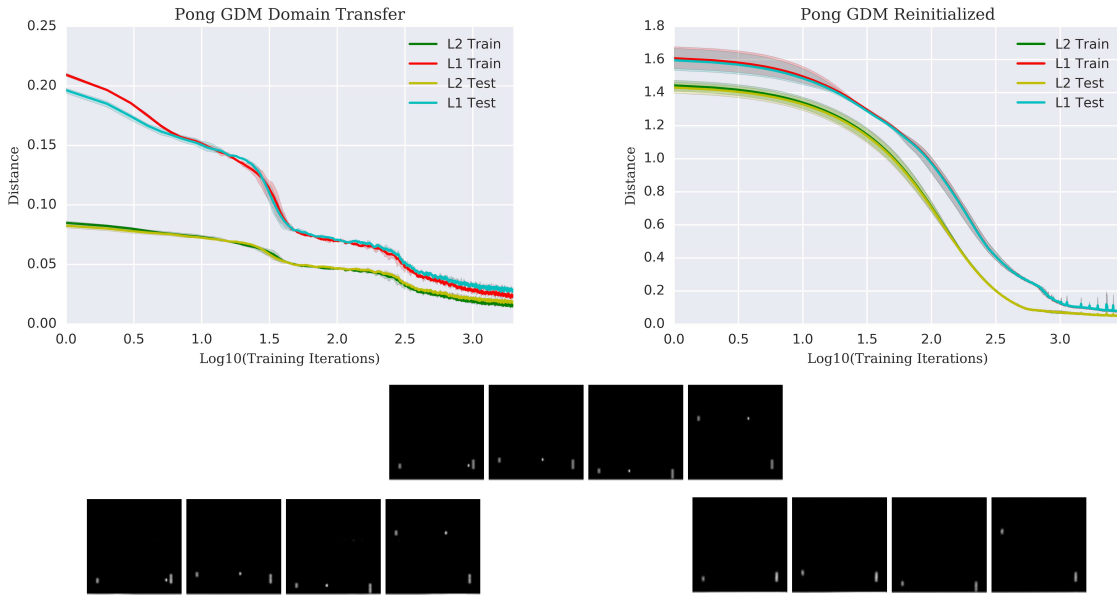


Figure 9: Training and evaluating domain transfer for GDM on new game dynamics for Pong (Mode 1, Difficulty 1). GDM domain transfer from Pong (Mode 0, Difficulty 0) on *left* and GDM from re-initialized parameters on *right*. L1 and L2 loss curves displayed *top*. Ground truth next frames displayed *middle* with predicted next frames displayed *bottom*.

GDM Domain Adaptation. We evaluate the GDM’s ability to perform domain adaptation using the environment mode and difficulty settings in the latest Arcade Learning Environment²⁹. We first fully train GDM and DDQN on Pong with Difficulty 0 and Mode 0. We then sample 10,000 frames for training the GDM on Pong with Difficulty 1 and Mode 1, which has a smaller paddle and different game dynamics. We also collect 10,000 additional frames for testing the GDM. We train GDM using transferred weights and reinitialized weights on the new environment samples and observe the L1 and L2 loss on training and test samples over approximately 3,000 training iterations, and we observe that they decrease together without significant over-fitting in Fig. 9. To qualitatively evaluate these frames, we plot the next frame predictions of four test images in Fig. 9. We observe that training GDM from scratch converges to a similarly low L1 and L2 loss quickly, but it fails to capture the game dynamics of the ball. This indicates the L1 and L2 loss are bad measurements of a model’s ability to capture game dynamics. GDM is very efficient at transfer. It quickly learns the new model dynamics and is able to generalize to new test states with an order of magnitude fewer samples than the Q -learner.

GDM Comparison Study. We experimented with many different model architectures for the generator and discriminator for GDM, as well as different loss functions. We compare performance visually on test samples, since the L1 and L2 losses are not good metrics for learning game dynamics as demonstrated in the previous paragraph and also Fig. 9. We experiment with the PatchGAN discriminator (patch sizes 1, 16, and 70) and $L1$ loss used in PIX2PIX¹⁹. We find this architecture takes approximately $10x$ more training iterations to learn game dynamics for Pong than GDM. This is likely since learning game dynamics such as ball position requires the entire frame for the discriminator, more than the patch-based texture loss given by PatchGAN. We also experiment with the ACVP³⁴ architecture for the generator trained on L2 loss using the same hyper-parameters as specified in the original paper, and we find it also takes an order of magnitude more training iterations to learn game dynamics. We hypothesize this is because ACVP is a much larger network optimized for long term predictions, and does not take advantage of skip-connections and the discriminative loss.

For the choice of the GAN loss, we first tried the original GAN-loss¹⁶ which is based on Jensen–Shannon distance. With this criterion, it is difficult find the right parameters but not stable enough for non-stationary domains. The training loss is unstable even for the given fixed data

set. Since, Wasserstein metric provides Wasserstein distance criterion and is a more general loss in GANs, we deployed W-GAN³ for our GDM. As W-GAN requires the discriminator to be bounded Lipschitz function, the authors propose the gradient clipping to make the W-GAN training stable and effective. Using W-GAN provided improvement, but still, was not sufficient for RL where fast and stable convergence is required. In order to improve the learning stability, parameter robustness, and quality of frames, we also tried the follow-up work on improved-W-GAN¹⁷ which adds a gradient penalty into the loss of discriminator in order to satisfy the bounded Lipschitzness. Even though it made the GDM more stable than before, it was still not sufficient due to the huge instability in the loss curve. Finally, we tried a new technique, called spectral normalization³², which not only provides high quality frames, but also converges quickly while the loss function stays smooth. Because of the stability, robustness to hyper parameters, and fast learning characteristics of spectral normalization combined with W-GAN, GDM is able to handle the change in the state distribution in RL and still preserve the frame quality.

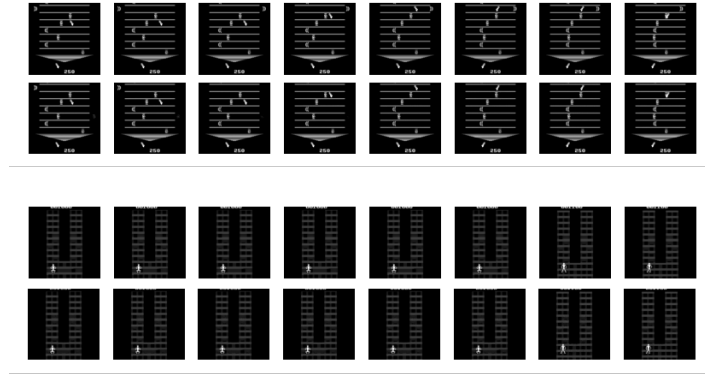


Figure 10: Sample 8-step GDM roll-outs on Atari 2600 gym domains: Asterix (top) and Crazy-Climber (bottom).

GDM Atari Evaluation. The GDM is able to learn model dynamics for many different Atari domains using the same model architecture and hyper-parameters. We train the GDM on a replay buffer of 100,000 training frames using a 3-step loss, and evaluate its performance on 8-step roll-outs from a test buffer of 10,000 frames. Actions are chosen at random. Sample 8-step roll-outs are shown in Figure 10.